

# Improved-Sensitivity Integral SQUID Magnetometry of (Ga,Mn)N Thin Films in Proximity to Mg-doped GaN

Katarzyna Gas,<sup>1,\*</sup> Gerd Kunert,<sup>2</sup> Piotr Dłuzewski,<sup>1</sup> Rafał Jakiela,<sup>1</sup> Detlef Hommel,<sup>2,3,4</sup> and Maciej Sawicki<sup>1</sup>

<sup>1</sup>*Institute of Physics, Polish Academy of Sciences,  
Aleja Lotników 32/46, PL-02668 Warsaw, Poland*

<sup>2</sup>*Institute of Solid State Physics, University of Bremen, Otto-Hahn-Allee 1, 28359 Bremen, Germany*

<sup>3</sup>*Institute of Experimental Physics, University of Wrocław, M. Born'a 9, Wrocław, Poland*

<sup>4</sup>*Lukasiewicz Research Network - PORT Polish Center for Technology Development, Stabłowicka 147, Wrocław, Poland*  
(Dated: December 23, 2024)

Nominally 45 nm GaN:Mg / 5 nm (Ga,Mn)N / 45 nm GaN:Mg trilayers structures prepared by molecular beam epitaxy on GaN-buffered Al<sub>2</sub>O<sub>3</sub> substrates are investigated to verify whether the indirect co-doping by holes from the cladding layers can alter the spin-spin interaction in (Ga,Mn)N. The four investigated structures, differing with the Mg doping level, are carefully characterized at the nanoscale by high-resolution transition electron microscopy (HRTEM), energy-dispersive X-ray spectroscopy, and by secondary ion mass spectrometry. Importantly, HRTEM decisively excluded a presence of foreign Mn-rich phases. The structures, up to medium Mg doping, show no Mg over-doping effects. Magnetic studies of these structures are aided by the employment of a dedicated experimental approach of the *in situ* compensation of the magnetic contribution from the substrate, allowing up to about fifty-fold reduction of this contribution. This technique, dedicated to these structures, simultaneously provides a tenfold reduction of temporal instabilities of the magnetometric unit and lowers the experimental jitter to merely  $5 \times 10^{-7}$  emu at 70 kOe, vastly increasing the precision and the credibility of the results of the standard integral superconducting quantum interference device (SQUID) magnetometry in high magnetic fields. The magnetic characteristics of the trilayers structures established here prove identical with the already known properties of the thick (Ga,Mn)N single layers, namely (i) the low temperature ferromagnetism among Mn<sup>3+</sup> ions driven by superexchange and (ii) purely paramagnetic response at higher temperatures. The possible cause of the lack of any effects brought about by the adjacent Mg-doping is a presence of residual Mn in the cladding layers, resulting in the deactivation of the p-type doping intended there. This finding points out that a more intensive technological effort has to be exerted to promote the co-doping-driven carrier-mediated ferromagnetic coupling in Mn-enriched GaN, especially at elevated temperatures.

Keywords: magnetic films and multilayers, nitride materials, semiconductors, crystal growth, magnetization, magnetic measurements

---

\* kgas@ifpan.edu.pl

## I. INTRODUCTION

Since the family of nitrides has reached the status of the second most important semiconducting class of materials after Si, the prospect of spintronics functionalization of GaN has gained significance. However, the most obvious way of magnetic functionalization of GaN, following the influential concept of Dietl and co-workers [1], by controlled incorporation of transition metals (mainly Mn), proved fruitless despite intensive efforts [2]. The prerequisite condition for the room temperature carrier mediated ferromagnetism is a *simultaneous* presence of a large concentration of *randomly* distributed substitutional Mn cations (at least 5%) and a comparably high concentration of mobile holes ( $3 \times 10^{20} \text{ cm}^{-3}$ ). Both requirements constitute a certain technological challenge on their own, combined have proved impossible to meet to date. Firstly, because of a rather low thermodynamic solid solubility limit of Mn in GaN ( $2 \times 10^{17} \text{ cm}^{-3}$  [3]) Mn atoms tend to agglomerate during the growth into various Mn-rich nano-precipitates nested in the paramagnetic host, exhibiting a wide spectrum of coupling temperatures and spin configurations [4]. This fact calls for an extensive and thorough nano-characterization effort, as the formed Mn-rich nanocrystals can dominate the magnetic properties, particularly at high temperatures. Although the recently elaborated bulk-oriented synthesis methods allow to surpass the solubility limit by two orders of magnitude [5–8], the obtained GaN:Mn crystals remain still another two orders of magnitude short to satisfy the mean field model requirements [1].

Therefore, the highest hopes to obtain a device viable material have been directed to non-thermal equilibrium growth methods, namely metal organic vapor phase epitaxy (MOVPE) and molecular beam epitaxy (MBE) techniques, where a substantial simultaneous Mn and p-type doping seem achievable. However, a direct co-doping of GaN with Mn and Mg (the industrially standard p-type dopant for GaN [9, 10]) at the same time led to the formation of Mn-Mg<sub>k</sub> complexes [11], or yielded unsettled results [2, 12]. To circumvent these obstacles, a range of structure designs were attempted to physically separate the Mn- and p-type doping. In the first class of attempts the effort was aimed at achieving an efficient carrier transfer across the (Ga,Mn)N/p-GaN interface to induce the ferromagnetic (FM) ordering in the former [13]. In the other one, the hole wave functions were expected to extend into (Ga,Mn)N to facilitate the FM coupling [14], extending up to 8-9 nm, i.e. well beyond the interfacial region [15]. Yet another approach relied on a geometrical confinement, so that a forced coexistence of both, the Mn species and the holes in (Ga,Mn)N based nanorods or nanowires was expected [16]. Again, also all of these approaches yielded rather conflicting results. However, it should be noted that in the latter case, a substantial strain specific to the nanowire geometry can substantially increase the Curie temperature of the embedded Mn-rich nanocrystals [17].

Due to the absence of any following extensive works reporting either an operational spintronic device or a magnetic phase diagram up to room temperature, it is reasonable to assume that high-temperature FM in GaN with Mn is not under control. Therefore, it remains likely that the observation of the reported high-temperature magnetic features signalizes an inhomogeneous distribution of Mn atoms formed by either coherent chemical separation or crystallographic phase precipitation. A very similar conclusion can be drawn from a very recent attempt to induce the high temperature FM in GaN by the delta doping ( $\delta$ -doping) method [18]. It should be noted, however, that in this case the claims about the above-room-temperature FM are partially based upon non-reproducible results related to unspecified instrumentation issues (c.f. Fig. 1 c of ref. [18]). Finally, it is also worth acknowledging the formidable challenges connected with an unambiguous analysis of the results obtained for magnetic layers grown by the  $\delta$ -doping method. A wide ranging and a truly in-depth structural characterization at the nanoscale of Fe  $\delta$ -doped GaN was required to unravel the form and chemical composition of Fe-rich nanocrystals coherent with the GaN lattice, whose weak magnetic signatures have been observed even beyond room temperature [19].

On the other hand, in single-crystalline (Ga,Mn)N epitaxial films with an experimentally documented random distribution of Mn atoms and a small concentration of compensating defects or impurities, clear FM features were found exclusively at low temperatures [20–22]. In the low temperature regime, the FM obeys a clear phase diagram and is so robust that the critical exponents for the paramagnetic-ferromagnetic phase transitions were experimentally

determined [23]. These layers are devoid of carriers [24, 25] and the Fermi level is pinned on the only partially filled  $\text{Mn}^{3+}$  level in the mid-gap region of GaN [26–28]. In the absence of carriers, the necessary Mn-Mn coupling is provided by superexchange. This major coupling mechanism in wide gap dilute magnetic semiconductors, which is known to be predominantly antiferromagnetic there, turns ferromagnetic for  $\text{Mn}^{3+}$  ions in tetrahedral configuration [29], i.e. in GaN. It is the short-range nature of this coupling mechanism which limits the Curie temperature  $T_C$  to a mere 10 K for currently maximum achievable  $x$  of 10%. Yet, the industrial importance of the nitride compounds, their current dominance in optoelectronic [30] and high-power applications [31] still holds the doors wide open for a technology-viable nitride semiconductor exhibiting robust magnetic properties above the room temperature.

In the study reported here, we put to the test the hypothesis whether the indirect p-type co-doping can stimulate an increase of the FM ordering temperature in single-phase (Ga,Mn)N. To this end a very thin (Ga,Mn)N layer is sandwiched between two thicker GaN:Mg layers to form a trilayer heterostructure. Since the (Ga,Mn)N layer is grown following our elaborated specifications, which routinely results in single-crystalline films of single-Kelvin coupling temperature [22, 23], any impact of the neighboring holes should yield a straightforward result. While keeping nominally the same growth parameters for the (Ga,Mn)N central layer, the magnitude of the Mg doping level in the cladding GaN:Mg is substantially varied. Yet it is kept sufficiently low not to induce polarity inversion and deterioration of the interface morphology [15]. The combined thorough structural characterization confirms crystallographically and magnetically single phase of (Ga,Mn)N and the desired layout of our heterostructures. A dedicated method of the *in situ* compensation of the signal from the substrate has been elaborated and actively employed for the magnetic measurements in our magnetometer [32]. The resulting, up to 50 fold, reduction of the contribution of the substrate allows to sizably increase the real resolution and the credibility of the results. Basing on these measurements any presence of the "FM-like" signal at elevated temperatures has been excluded – the layers are found to exhibit purely paramagnetic response at  $T \geq 50$  K. Conversely, clear FM features are found only below about 6 K with the main attributes identical to those already known of the thick (Ga,Mn)N single layers. Our experimental effort univocally proves that the presence of the adjacent GaN:Mg layers has not influenced the spin-spin interactions in the central (Ga,Mn)N. The unique for such structures nano characterization effort points to the presence of a residual Mn in the cladding GaN:Mg layers. It is argued that this astray Mn is the most likely culprit responsible for the lack of Mg-doping effect. This findings indicates that a more intensive technological effort is needed to break the deadlock in the effectiveness of the simultaneous Mn- and Mg-codoping in GaN, when an increase of the strength of the spin-spin coupling in (Ga,Mn)N is targeted.

## II. EXPERIMENTAL

### A. Sample growth

The nominally (45 nm) / (5 nm) / (45 nm) trilayer heterostructures GaN:Mg / (Ga,Mn)N / GaN:Mg investigated here are grown by MBE technique in an EPI 930 MBE chamber on fully relaxed GaN templates (thickness  $\sim 2\mu\text{m}$ ) fabricated by MOVPE on *c*-plane 0.3 mm thick  $\text{Al}_2\text{O}_3$  substrates. Radio-frequency nitrogen plasma source operating at a power of 300 W is used and is set to give the nitrogen flux of 1.3 sccm. Suitable growth parameters for interfaces between GaN:Mg and (Ga,Mn)N, precluding polarity inversion from originally Ga-face to N-face GaN were determined in earlier studies [15]. During the growth of both materials metallic films form on the surface. To create sharp interfaces between the layers of different doping, the metallic films are evaporated by a 700 s growth break at the relevant growth temperatures. The magnetic  $\text{Ga}_{1-x}\text{Mn}_x\text{N}$  middle layers are fabricated with standard growth parameters calibrated to obtain Mn concentration,  $x$ , of about 5% on undoped GaN/ $\text{Al}_2\text{O}_3$ , i.e. at the growth temperature  $T_g = 730^\circ\text{C}$  [10]. The Mg content in the GaN:Mg cladding layers is varied by changing the Mg flux ( $\Phi_{\text{Mg}}$ ) from 0, through  $7 \times 10^{-9}$  (low, L) and  $1 \times 10^{-8}$  (medium, M) to  $2 \times 10^{-8}$  (high, H) Torr beam equivalent pressure (BEP). All the cladding layers

are grown at the same 730°C growth temperature and a Ga flux of  $2 \times 10^{-6}$  Torr BEP. For the (Ga,Mn)N layers, the Ga flux is  $8.5 \times 10^{-7}$  Torr BEP, with the Mn flux set to  $1 \times 10^{-6}$  Torr BEP. Structures are labeled according to the intensity of  $\Phi_{\text{Mg}}$  and listed in Table I.

TABLE I. Data related to the investigated GaN:Mg / Ga<sub>1-x</sub>Mn<sub>x</sub>N / GaN:Mg trilayers. The sample codes indicate the intensity of the Mg flux used to grow either of the cladding GaN:Mg layers. The columns display the magnitudes of the Mg flux ( $\Phi_{\text{Mg}}$ ), Mn content, ( $x$  - obtained from magnetization data), Mg concentration ( $n_{\text{Mg}}$ ) established by secondary ion mass spectrometry, and Curie temperature  $T_{\text{C}}$ .

Sample code	$\Phi_{\text{Mg}}$ [ $10^{-8}$ Torr BEP]	$x_{\text{Mn}}$ [%] ( $d = 4.3$ nm)	$n_{\text{Mg}}$ [ $10^{20}$ cm $^{-3}$ ]	$T_{\text{C}}$ [K] $\pm 0.5$ K
S <sub>0</sub>	—	$4.5 \pm 0.6$	0.003	2.6
S <sub>L</sub>	0.7	$6.4 \pm 0.8$	3	3.5
S <sub>M</sub>	1.0	$4.0 \pm 0.5$	4	4.1
S <sub>H</sub>	2.0	$0.2 \pm 0.2$	9	< 2

### B. Structural characterization

The structural characterization is performed using FEI Titan 80-300 Cubed Cs image corrected transition electron microscope (TEM) operated at 300 kV and equipped with Energy-dispersive X-ray spectroscopy (EDX) spectrometer. The cross-sectional lamellas for TEM are prepared by FIB technique with Pt as a protected capping layer. Element specific depth profiling is performed by secondary ion mass spectrometry (SIMS) using a CAMECA IMS6F microanalyzer.

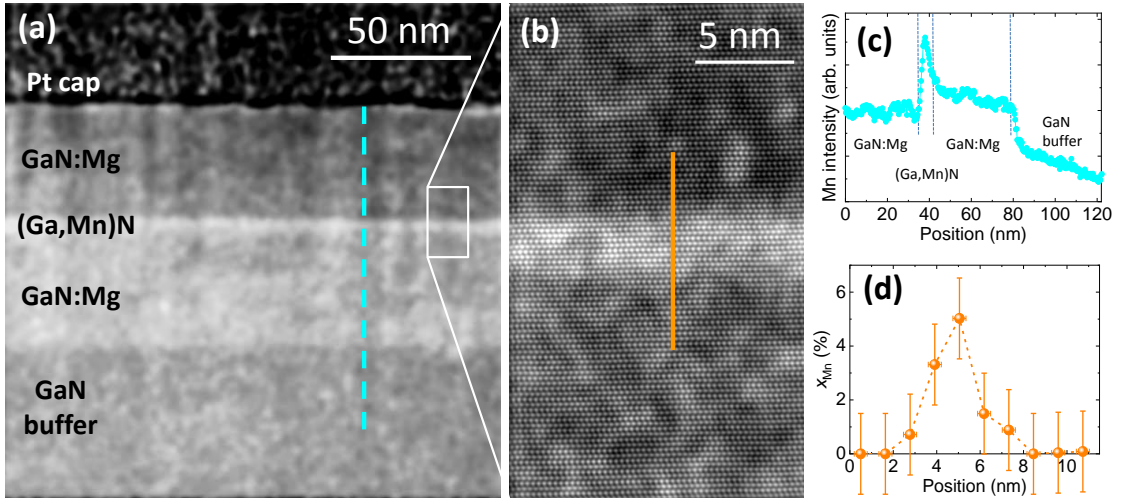


FIG. 1. (Color on line) (a) An example of cross-sectional transmission electron microscopy (TEM) image of the S<sub>M</sub> structure (detailed in Table I). The Mn-containing layer is running horizontally through the image between GaN:Mg ones. (b) High resolution TEM close up into the (Ga,Mn)N layer and its vicinity. (c) Energy-dispersive x-ray spectroscopy (EDX) established Mn concentration scan along the dashed cyan line indicated in (a). (d) EDX-established Mn concentration scan along the orange line indicated in (b).

The accurateness of the obtained heterostructures is confirmed in Fig. 1, taking the S<sub>M</sub> structure as the sole representative. As shown later, this sample exhibits the strongest magnetic response, and so it constitutes the key

element to formulate the final conclusions of this study. The TEM image in Fig. 1 (a) confirms the trilayer's intended design and a general high quality of the obtained material. Some incidental defects have been detected, but they are clearly associated with dislocations propagating from the buffer / substrate interface to the free surface. This is the characteristic feature of the heteroepitaxy of GaN on  $\text{Al}_2\text{O}_3$  and so is not presented here. The high-resolution (HR) images, as the one in Fig. 1 (b) reveal the high quality crystal structure of (Ga,Mn)N and a high quality of the interfaces. The HR images also allow to determine the (Ga,Mn)N layer thickness,  $d$ . It is found to range between 3.8 and 4.8 nm (16 to 18 the 00.2 monolayers), and a final value of  $d = (4.3 \pm 0.5)$  nm has been adopted for all the structures. The uncertainty of  $d$  given here constitutes the main contribution determining the magnitude of error in the determination of  $x$  from magnetic measurements. According to cross-section EDX measurements,  $x$  in the middle of the layer does not exceed 5%, Fig. 1 (c), but the concentration profile assumes rather a bell-like shape than required rectangular one in the expected location of the (Ga,Mn)N layer. Given a rather substantial uncertainty of this method, we accept this result as another solid confirmation of the correctness of the growth. More importantly, basing on the overall HRTEM effort exemplified in Fig. 1, we confirm the single-phase character of the investigated multilayers, i.e. the TEM studies excluded the presence of any secondary crystalline phases or Mn aggregations.

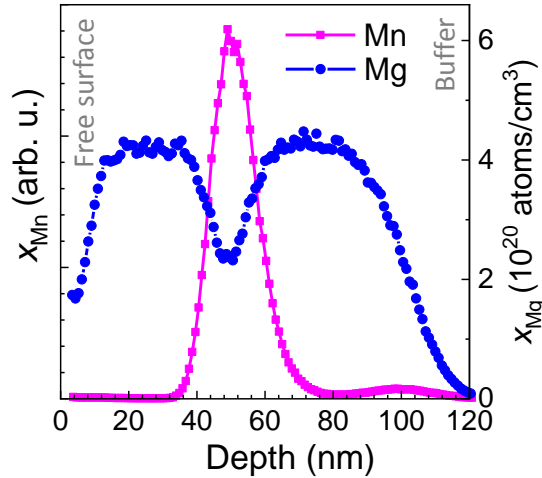


FIG. 2. (Color on line) Secondary ion mass spectrometry (SIMS) Mn- and Mg-depth profiles of the  $S_M$  structure (grown with the medium Mg flux of  $1 \times 10^{-8}$  Torr BEP). An apparently larger width of the (Ga,Mn)N layer in SIMS than in TEM study is the method's artefact due to mixing/segregation mechanism specific for SIMS measurements [33].

The intended Mn and Mg doping profile is further confirmed by SIMS, exemplified in Fig. 2 for the same sample  $S_M$ . We confirm that all four structures exhibit qualitatively identical profiles. SIMS studies confirm that the thin (Ga,Mn)N layer is sandwiched between two, uniformly doped, about 40 nm thick GaN:Mg layers. The few nm smearing is a typical technique-related artefact originating in mixing and segregation mechanisms [33]. The established Mg doping levels,  $n_{\text{Mg}}$ , for each of the samples are listed in Table I. It varies from  $3 \times 10^{17} \text{ cm}^{-3}$  for the sample grown with no Mg flux ( $S_0$ ) to  $9 \times 10^{20} \text{ cm}^{-3}$  for the structure grown under high Mg flux ( $S_H$ ).

Importantly, both TEM and SIMS techniques detect some Mn outdiffusion from its intended nesting place. A clear difference in brightness of both GaN:Mg cladding layers are seen in the image in Fig. 1 (a). Additional, about 120 nm EDX vertical scan through the cross-sectional image in Fig. 1 (a) univocally points to non-zero Mn concentration in the cladding layers, particularly in comparison to the GaN buffer layer. The recorded Mn level is higher in the "lower" layer, i.e. the one which was grown first. The same effect is evidenced by SIMS as a weak yield of Mn signal at the region corresponding to the beginning of the growth of the whole trilayer structure.

### C. Magnetic measurements and discussion

It should be remarked here that for such very thin layers of a highly dilute compound, both EDX and SIMS techniques can only be regarded as qualitative probes when it comes to determination of the concentration of the magnetic species. In order to quantitatively assess the magnitude of  $x$  in the (Ga,Mn)N layers, we resort to the magnetic measurements, which allow to establish  $x$  from the magnitude of the low temperature saturation magnetization,  $M_{\text{Sat}}$ . However, taking into account a rather slowly saturating magnetization,  $M$ , in (Ga,Mn)N and the documented existence of a sizable magnetic anisotropy, MA [34–36], a rather strong magnetic field of few tens of kOe is required [34, 37–39], what makes the whole undertaking very challenging.

We start from the notion that for the technological parameters of our (Ga,Mn)N mid-layer the saturation magnetic moment of a  $5 \times 5 \text{ mm}^2$  piece at 2 K and 70 kOe should amount to about  $8 \mu\text{emu}$ . From one side this value safely exceeds the declared sensitivity of commercial SQUID magnetometers by two orders of magnitude, but from the other, it is only 1% of the diamagnetic signal exerted at the same time by an equivalent 0.3 mm thick sapphire substrate. Therefore, an exceptional care and adequateness of the experimental procedures have to be enforced to eliminate artifacts and evade limitations associated with the integral SQUID magnetometry [40, 41]. In the case of this study a correct determination of the magnetic contribution brought about by the substrate is the most important factor determining the credibility of the final results and in turn of the whole effort.

Unfortunately, the ubiquitously assumed "ideally diamagnetic" response of even the cleanest sapphire substrates, and of other substrate materials, is not at all linear in  $H$  and  $T$ -independent. In the authors' view, such a groundlessly assumed ideal diamagnetic response should also be regarded as a very significant source of the so frequently reported "room temperature ferromagnetism" in GaN:Mn and similar systems. In this context, the following two leading contributions should be mentioned. Firstly, these are the residues of the metallic glue or substrate backside metallization used to attach and thermalize the substrates in the growth chambers. This stuff has to be meticulously removed before the measurements. Secondly, magnetically active contaminants present in the bulk of the substrate must be mentioned. In the case of sapphire, this surplus "magnetism" is predominantly caused by Cr [42], but other transition metals are likely to be present, too. Therefore, and unfortunately, the magnetic purity of substrates does vary from vendor to vendor and it fluctuates in long runs in time, even when the material is acquired from the same source. It is therefore imperative that only the best, preselected batches of the substrates should be used when magnetic measurements are expected. However, the best does not mean the ideal. An extra nontrivial  $T$ - and  $H$ -dependent contributions to the measured magnetic moment  $m(T, H)$  are always present. The existence of this detrimental contribution of the non-linear and hysteretic  $m(T, H)$  of sapphire has been already exemplified in ref. 34 and in the Supplementary Information part of ref. [32]. These examples convincingly illustrate the existence of a deceivingly FM-like nonlinear magnetic response in epi-ready sapphire substrates. Treating this response as originating from a hypothetical 5 nm thin (Ga,Mn)N layer, i.e. assuming the ideally diamagnetic response of the sapphire, one would readily obtain  $x$  as high as 7 – 10% from the low temperature data [Fig. S1 (b) of ref. [32]]. Most importantly, basing on the high- $T$  data presented in Fig. S2 (a) of ref. [32] one could enthusiastically declare an existence of a RT FM with the saturation magnetization in the range between  $0.6 - 1 \mu_B/\text{Mn}$ .

In order to mitigate these issues and so to vastly increase the credibility of our magnetic investigation, a special *in situ* substrate-compensating experimental method was elaborated. Both, a special (substrate) compensational sample holder (CSH) has been prepared and the adequate experimental routine has been developed [32]. The actual CSH used here is presented in Fig. 4 (c) in ref. [32]. The compensating strips were cut from a 2" sapphire wafer originating from the same batch of wafers used to grown the structures studied here. Accordingly, all the results presented below are substantially devoid of any magnetic contributions not-specific to the (Ga,Mn)N layers of interest. This method, as a whole undertaking, constitutes a vast experimental advancement not only because the signal of a particular substrate can be compensated down to a single % level. It also provides a tenfold reduction of the temporal instabilities of

the magnetometric unit, which are detrimental for the precise magnetometry. At the same time the method lowers the experimental jitter to a mere  $5 \times 10^{-7}$  emu at 70 kOe. The same approach has also proved particularly useful in investigations of other systems exhibiting minute magnetic signals, i.e. magnetic nanocrystals [19, 43, 44], and very thin antiferromagnetic layers [45, 46].

The magnetic measurements are performed using a Quantum Design MPMS XL-7 Superconducting Quantum Interference Device (SQUID) magnetometer between 2 and 300 K and up to 70 kOe. For the studies the material is diced into  $5 \times 5$  mm<sup>2</sup> specimens, which for detailed orientation-dependent studies are further cut into four  $\sim 1.2$  mm wide strips. The experimental material is extracted from the center of the wafers to minimize the inhomogeneity of the Mn doping caused by an inevitable temperature inhomogeneity over the substrate surface during the MBE growth [39, 47]. Before the measurements, the pieces are bathed in HCl for about 30 mins in an ultrasonic cleaner to remove any metallic contaminants. The strips are then glued together to form a cuboid of a square cross-section  $(1.2 \times 1.2 \times 5)$  mm<sup>3</sup>, as detailed in ref. [35]. Magnetic studies in both, in-plane and perpendicular orientation are performed by a 90° rotation of such a cuboidal sample along its length. This is done without a noticeable change of the sample to SQUID-pick-up-coil coupling factor  $\gamma$ . For a typical  $5 \times 5$  mm<sup>2</sup> sized sample  $\gamma$  differs between these two orientations by as much as 5% [40, 48]. So, the possible change of the signal specific to the substrate alone due to such a change of  $\gamma$  exceeds about 5 times the expected magnitude of the magnetic response of (Ga,Mn)N layers investigated here.

The near zero-magnetic-field conditions, which are required to determine the magnitude of the Curie temperature  $T_C$ , are established by a careful degaussing of the superconducting magnet of the magnetometer. This is done by applying a slowly oscillating magnetic field with decreasing amplitude and is followed by the soft quench. As established separately by measuring a pellet of a strong paramagnetic salt (Dy<sub>2</sub>O<sub>3</sub>) the typical magnitude of  $H$  in the sample chamber does not exceed 0.12 Oe after this procedure. As reasoned before, all the measurements are performed using the dedicated CSH [32].

An example of the development of the magnetic response of the heretostructures studied here is given for sample S<sub>M</sub> in Fig. 3. The magnetic field dependence of the magnetization  $M$ ,  $M(H)$ , in the wide field range at 2, 5, 50 and 300 K is presented in panel (a). It is clearly seen that at the two highest temperatures the signal is paramagnetic, showing no tendency towards saturation in the whole available range of  $H$ . Most importantly, no FM-indicative features, like a non-zero remnant magnetization or nonlinearities of  $M(H)$  are observed there. This is the common behavior found in all the studied samples. It confirms that neither ferromagnetic Mn-enriched clusters are present in these structures nor a carrier induced room temperature ferromagnetism has been induced. The intimate proximity of the (Ga,Mn)N to the Mg-doped cladding layers has not resulted in any qualitative change of the magnetic character of the (Ga,Mn)N material researched here.

Conversely, at the low- $T$  end, in agreement to the previous studies [20–23, 25, 36, 39],  $M(H)$  acquires a clear sigmoidal shape and the magnetic saturation is evidenced above 40 kOe at 5 K and around 20 kOe at 2 K. This behavior is indicative that a FM scenario does take place here, but only at these lowest temperatures. A vital clue about the possible nature of this coupling comes from the magnetic anisotropy data presented in Fig. 3 (b). The most important feature in this graph is the easy-plane character of MA. This behavior decisively rules out a statistically significant presence of Mn ions in +2 oxidation state, as this orbital singlet state is isotropic and its spin couples antiferromagnetically with the neighbors [38, 49, 50]. Therefore, on the account of the accumulated body of evidences in the low to medium doped (Ga,Mn)N, i.e. for  $x$  not greater than several % [23, 25, 36, 38, 39], the combined data presented in Fig. 3 constitute the telltale evidence of the prevalence of the Mn<sup>3+</sup> state of Mn ions in the (Ga,Mn)N layer. In such a case the magnetic superexchange is the driving mechanism for the FM witnessed here [29, 51–53].

Having established the dominant Mn oxidation state in our layers, the Mn concentration can be determined using the crystal field model (CFM) relevant for Mn<sup>3+</sup> [34, 37, 38, 54–59]. The direct CFM computations for noninteracting Mn<sup>3+</sup> cations yield that the near-saturation value at 70 kOe and 2 K is  $3.78 \mu_B$  per Mn ion [34, 36, 37]. The

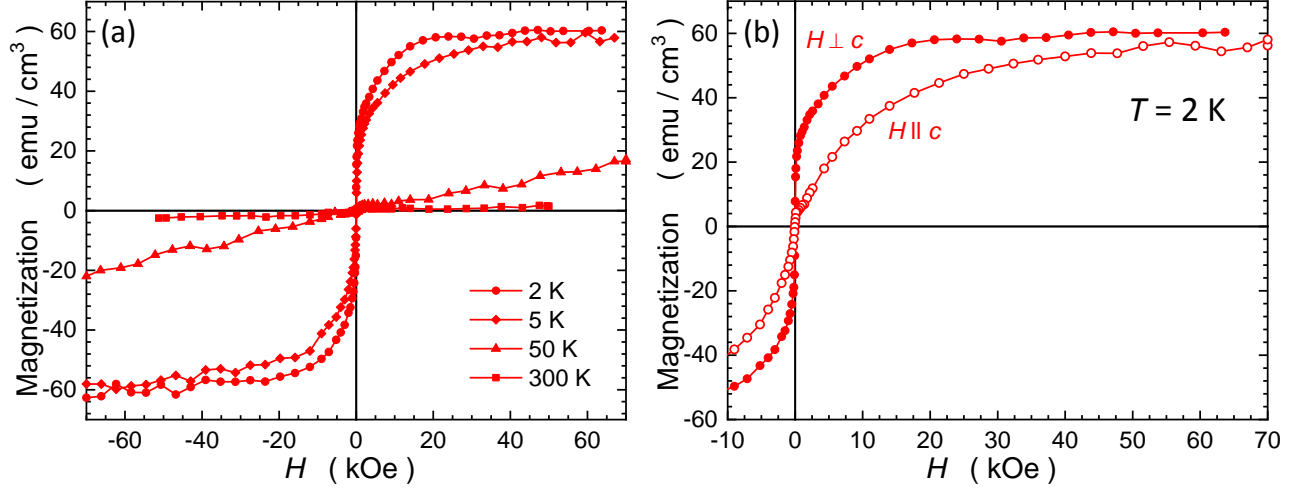


FIG. 3. (Color on line) Isothermal magnetization curves  $M(H)$  specific to the central (Ga,Mn)N layer from structure  $S_M$  measured for the in-plane magnetic field  $H$  orientation at 2, 5, 50 and 300 K and (b) at 2 K for both in-plane (solid symbols) and perpendicular (open symbols) orientations of  $H$ . The former orientation corresponds to  $H$  perpendicular to the wurtzite  $c$  axis,  $H \perp c$ , the latter to  $H$  parallel to  $c$ ,  $H \parallel c$ , as labeled in the figure. The typical magnitudes of the error bars specific for the  $M(H)$  measurements are for clarity of the presentation exemplified in the next figure.

recently elaborated extension of this approach, which includes the near-neighbour coupling up to the clusters of four  $\text{Mn}^{3+}$  ions, does not affect the saturation level substantially [36]. Taking into account the details of the statistical distribution specific for different-size groups of Mn ions in a 5% wurtzite crystal [60], one finds that the saturation level increases only to  $3.79 \mu_B$ . Acknowledging, that in fact the main error in the determination of  $M_{\text{Sat}}$  originates from a large, about 20%, uncertainty of the (Ga,Mn)N layer thickness, the single ion figure has been adopted, as it is  $x$ -independent.

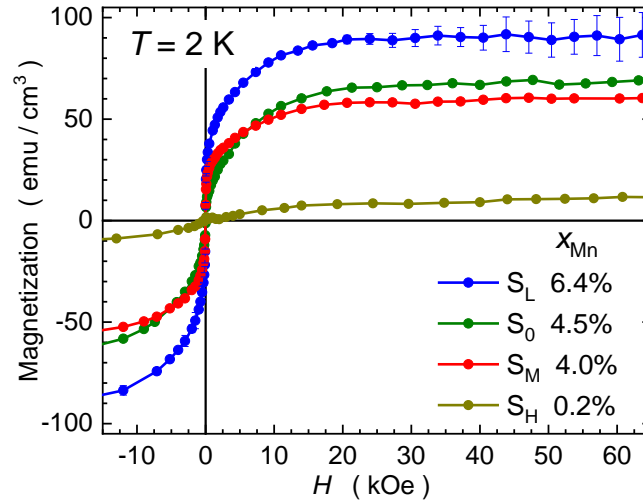


FIG. 4. (Color on line) Isothermal in-plane magnetization curves for all investigated structures measured at 2 K. The established saturation levels are used to calculate Mn concentration assuming nominal layer thickness of 4.3 nm and  $\text{Mn}^{3+}$  state of Mn ions, i.e. exhibiting saturation at  $3.79 \mu_B/\text{Mn}$  [36]. For clarity experimental errors are indicated only for one sample.

$M(H)$  curves collected at 2 K for the samples and so the magnetic saturation levels are given in Fig. 4. The resulting magnitudes of  $x$  are listed in the legend and in Table I. While the magnitude of  $x$  for three of the layers stays



at similar level between 4 and 6.4%, the low value established for  $S_H$  layer indicates that the Mg flux of  $2 \times 10^{-8}$  Torr BEP proves too intensive to incorporate Mn in the successive layer in an appreciable quantity. This goes in line with previous finding reported by Tropf *et al.* [15].

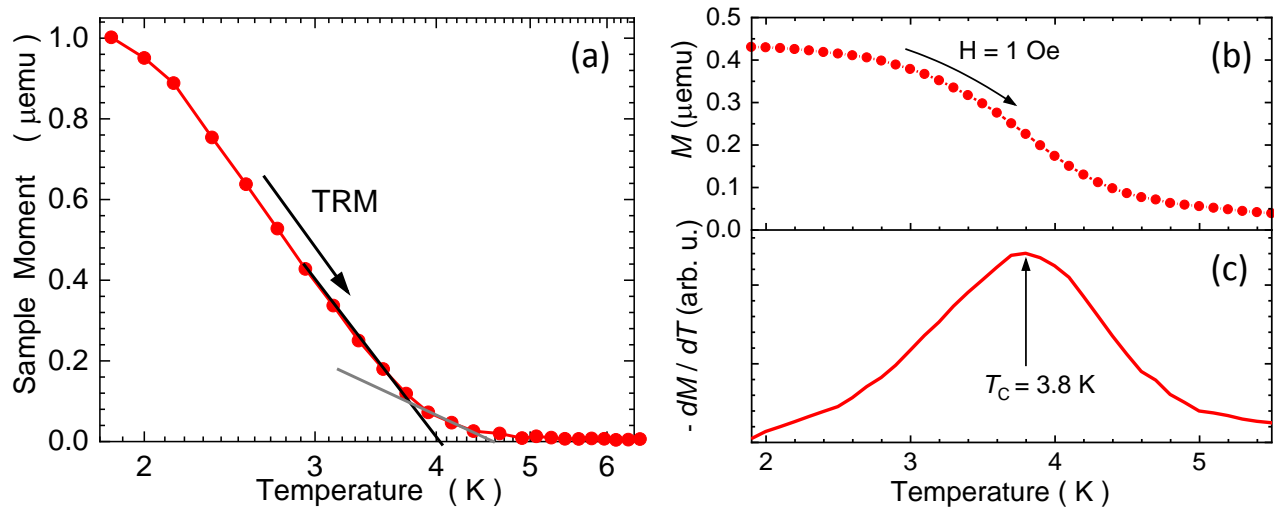


FIG. 5. (Color on line) Critical behavior of sample  $S_M$  and the Curie point determination from (a) thermoremanent magnetization (TRM) and (b) from the position of the inflection point on the temperature dependence of magnetization  $M(T)$ . In panel (a) the two lines indicate two possible methods of the interpolation of TRM to zero. They yield the lower and the upper bound limits of  $T_C$  from this method. The magnitude of the inflection temperature is obtained from the position of a maximum on numerically computed  $-dM(T)/dT$ , presented in panel (c). The  $M(T)$  dependency is measured at  $H = 1$  Oe.

Curie temperature of the (Ga,Mn)N layers is determined by two different methods employed previously [23, 39]. In either case, before the measurement, the superconducting magnet of the magnetometer is degaussed following the recipe given previously. In the first approach, the sample is cooled down from room temperature to the base temperature of  $T = 1.8$  K in  $H = 1$  kOe. Then, the magnetic field is quenched using the soft quench of the superconducting magnet. Under these conditions, the thermoremanent moment (TRM) is collected on increasing temperature until it drops to zero (that is, decidedly below the noise level). This temperature is understood to represent  $T_C$  of the system. The example of the TRM trace for sample  $S_M$  is depicted in Fig. 5 (a). A clear signal is seen at the base temperature, whereas at the transition region (between 4 and 4.8 K) the disappearance of TRM is not particularly abrupt. This smearing of the transition is a characteristic feature of dilute ferromagnets with randomly distributed magnetic species coupled in a percolation fashion via a short-range coupling. The formation of the FM state below the percolation limit (about 18%) is facilitated in only a few per cent (Ga,Mn)N by (i) exclusively positive values of the spin-spin coupling constants (at least up to the 16th neighbor [61]), and by (ii) a power-law decay of the exchange constant with distance. The process of the extrapolation TRM to zero can be aided by plotting the TRM data in the  $\log(T)$  scale. From the two "free hand" interpolation examples presented in Fig. 5 (a) we obtain  $4 < T_C < 4.6$  K.

In the second method, exemplified in Fig. 5 (b)  $T_C$  is determined from the inflection point of the  $M(T)$  dependency. It is measured at a very low field,  $H = 1$  Oe, and the inflection temperature is determined from the position of a maximum of electronically computed  $-dM/dT$ , as shown in Fig. 5 (c). This method yields  $T_C = 3.8 \pm 0.3$  K. For further quantitative analysis of the magnetic results we take the average of these two magnitudes with an error bar reflecting the maximum spread of the possible  $T_C$  values. In the case of the  $S_M$  sample  $T_C = 4 \pm 0.5$  K. All the  $T_C$  values are listed in Table I.

The magnetic characteristics of the (Ga,Mn)N layer determined in this study are summarized in the magnetic phase diagram presented in Fig. 6. The background data (gray symbols) are taken from ref. [23]. Only three samples with

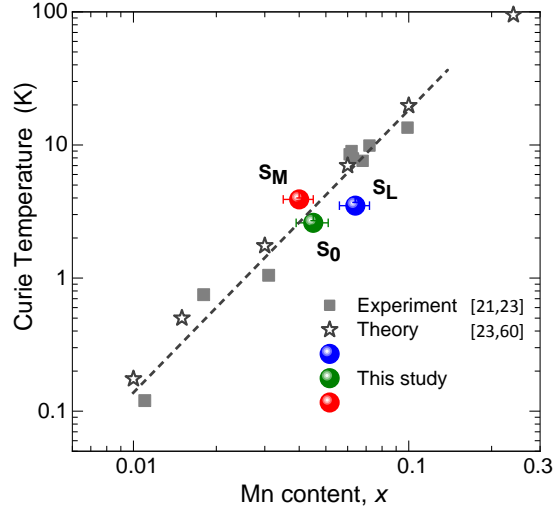


FIG. 6. (Color on line) Experimentally found Curie temperatures of the layers studies here (bullets) located on the background of (Ga,Mn)N magnetic phase diagram (gray symbols) [23]. Full squares represent experimental points, stars - results of Monte Carlo simulations with exchange integrals from the tight-binding model. The dashed line is a guide to the eye.

$T_C$  lying in the experimentally available  $T$ -range,  $T \geq 2$  K, are presented there. We find that these layers group very close to the trend established for thick single (Ga,Mn)N layers, fabricated just on GaN-buffered sapphire. This finding indicates that our attempt to augment the FM spin-spin coupling by placing the (Ga,Mn)N layer with the intimate contact with Mg-doped GaN has not resulted in any change of the already known magnetic properties of this material. The most likely reason for an unaltered magnetic picture found here is attributed to the presence of residual Mn in the Mg-doped layers. This is evidenced in Figs. 1 and 2. Acting as deep traps, the Mn species deactivate hole states formed by the Mg-doping. Indeed, the doping with Mn has become one of the most promising methods to produce industry standard semi-insulating bulk GaN substrates for high power and high frequency electronics [8, 62]. Mn doping levels as low as  $2 \times 10^{17} \text{ cm}^{-3}$  has been proved sufficient to produce highly resistive GaN even at room temperature [63].

### III. CONCLUSIONS

Specially designed GaN:Mg / (Ga,Mn)N / GaN:Mg structures on GaN-buffered  $\text{Al}_2\text{O}_3$  substrates have been grown by molecular beam epitaxy method following state-of-the-art growth protocols, aiming at an altering of the magnetic spin-spin interaction in the (Ga,Mn)N layer by the indirect co-doping by holes from the cladding layers. The four structures prepared for this study have been carefully structurally characterized. The structures with the none to medium Mg doping level showed no effects characteristic to Mg over-doping and the presence of any foreign Mn-rich phases has been decisively excluded. To eliminate spurious sources of the magnetic signals from the substrates, a dedicated experimental approach has been applied increasing both, the credibility and the sensitivity of the integral magnetometry at strong magnetic field. The magnetic characteristics proved identical to the already known properties of the thick (Ga,Mn)N single layers, the superexchange driven low temperature ferromagnetism and purely paramagnetic response above. The possible cause of the lack of any effects brought about by the adjacent Mg-doping is a presence of residual Mn in the cladding layers, resulting in the deactivation of the p-type doping intended there. This finding points out on the existing technological challenge lying ahead of such, or similar, attempts aiming at inducing a carrier mediated ferromagnetic coupling in GaN, especially at elevated temperatures.

## DECLARATION OF COMPETING INTEREST

The authors declare that they have no known competing financial interests or personal relationships that could have appeared to influence the work reported in this paper.

## ACKNOWLEDGMENTS

All authors contributed to the preparation of the draft of the manuscript and read, commented and corrected its final version. The work has been supported by the National Science Centre (Poland) through project OPUS 2018/31/B/ST3/03438.

- 
- [1] T. Dietl, H. Ohno, F. Matsukura, J. Cibert, and D. Ferrand, *Science* **287**, 1019 (2000).
  - [2] T. Dietl, K. Sato, T. Fukushima, A. Bonanni, M. Jamet, A. Barski, S. Kuroda, M. Tanaka, P. N. Hai, and H. Katayama-Yoshida, *Rev. Mod. Phys.* **87**, 1311 (2015).
  - [3] R. Jakiela, K. Gas, M. Sawicki, and A. Barcz, *Journal of Alloys and Compounds* **771**, 215 (2019).
  - [4] M. Zajac, J. Gosk, E. Grzanka, M. Kamińska, A. Twardowski, B. Strojek, T. Szyszko, and S. Podsiadlo, *J. Appl. Phys.* **93**, 4715 (2003).
  - [5] J. García, D. González, J. Bartolomé, R. Navarro, and J. Rojo, *Journal of Magnetism and Magnetic Materials* **51**, 365 (1985).
  - [6] I. Pop, M. Andreucut, I. Burda, R. Munteanu, and K. Criveanu, *Materials Chemistry and Physics* **37**, 52 (1994).
  - [7] H. Niida, T. Hori, H. Onodera, Y. Yamaguchi, and Y. Nakagawa, *Journal of Applied Physics* **79**, 5946 (1996), <https://aip.scitation.org/doi/pdf/10.1063/1.362115>.
  - [8] M. Zajac, R. Kucharski, K. Grabianska, A. Gwardys-Bak, A. Puchalski, D. Wasik, E. Litwin-Staszewska, R. Piotrkowski, J. Z Domagala, and M. Bockowski, *Progress in Crystal Growth and Characterization of Materials* **64**, 63 (2018).
  - [9] S. Nakamura, S. Pearton, and G. Fasol, “p-type GaN,” in *The Blue Laser Diode: The Complete Story* (Springer Berlin Heidelberg, Berlin, Heidelberg, 2000) pp. 113–147.
  - [10] A. Feduniewicz, C. Skierbiszewski, M. Siekacz, Z. Wasilewski, I. Sproule, S. Grzanka, R. Jakiela, J. Borysiuk, G. Kamler, E. Litwin-Staszewska, R. Czernecki, M. Boćkowski, and S. Porowski, *Journal of Crystal Growth* **278**, 443 (2005), 13th International Conference on Molecular Beam Epitaxy.
  - [11] T. Devillers, M. Rovezzi, N. Gonzalez Szwacki, S. Dobkowska, W. Stefanowicz, D. Sztenkiel, A. Grois, J. Suffczyński, A. Navarro-Quezada, B. Faina, T. Li, P. Glatzel, F. d’Acapito, R. Jakiela, M. Sawicki, J. A. Majewski, T. Dietl, and A. Bonanni, *Sci. Rep.* **2**, 722 (2012).
  - [12] M.-C. Jeong, M.-H. Ham, J.-M. Myoung, and S. K. Noh, *Applied Surface Science* **222**, 322 (2004).
  - [13] F. E. Arkun, M. J. Reed, E. A. Berkman, N. A. El-Masry, J. M. Zavada, M. L. Reed, and S. M. Bedair, *Appl. Phys. Lett.* **85**, 3809 (2004).
  - [14] N. Nepal, M. O. Luen, P. Frajtag, J. Zavada, S. M. Bedair, and N. El-Masry, *MRS Proceedings* **1198**, 119806E07 (2009).
  - [15] L. Tropic, G. Kunert, R. Jakiela, R. Wilhelm, S. Figge, J. Grenzer, and D. Hommel, *Journal of Crystal Growth* **437**, 49 (2016).
  - [16] Y.-T. Lin, P. V. Wadekar, H.-S. Kao, Y.-J. Zheng, Q. Y.-S. Chen, H.-C. Huang, C.-M. Cheng, N.-J. Ho, and L.-W. Tu, *Nanoscale Research Letters* **12**, 287 (2017).
  - [17] A. Kaleta, S. Kret, K. Gas, B. Kurowska, S. B. Kryvyi, B. Rutkowski, N. G. Szwacki, M. Sawicki, and J. Sadowski, *Nano Letters* **19**, 7324 (2019).
  - [18] P. V. Wadekar, Y.-T. Lin, C.-M. Lin, C.-W. Chang, Q. Y.-S. Chen, T.-C. Leung, C.-M. Cheng, and L.-W. Tu, *Journal of Alloys and Compounds* **834**, 154892 (2020).
  - [19] A. Navarro-Quezada, K. Gas, T. Truglas, V. Bauernfeind, M. Matzer, D. Kreil, A. Ney, H. Groiss, M. Sawicki, and A. Bonanni, *Materials* **13** (2020), 10.3390/ma13153294.
  - [20] E. Sarigiannidou, F. Wilhelm, E. Monroy, R. M. Galera, E. Bellet-Amalric, A. Rogalev, J. Goulon, J. Cibert, and H. Mariette, *Phys. Rev. B* **74**, 041306(R) (2006).

- [21] M. Sawicki, T. Devillers, S. Gałęski, C. Simserides, S. Dobkowska, B. Faina, A. Grois, A. Navarro-Quezada, K. N. Trohidou, J. A. Majewski, T. Dietl, and A. Bonanni, *Phys. Rev. B* **85**, 205204 (2012).
- [22] G. Kunert, S. Dobkowska, T. Li, H. Reuther, C. Kruse, S. Figge, R. Jakiela, A. Bonanni, J. Grenzer, W. Stefanowicz, J. v. Borany, M. Sawicki, T. Dietl, and D. Hommel, *Appl. Phys. Lett.* **101**, 022413 (2012).
- [23] S. Stefanowicz, G. Kunert, C. Simserides, J. A. Majewski, W. Stefanowicz, C. Kruse, S. Figge, T. Li, R. Jakiela, K. N. Trohidou, A. Bonanni, D. Hommel, M. Sawicki, and T. Dietl, *Phys. Rev. B* **88**, 081201(R) (2013).
- [24] T. Yamamoto, H. Sazawa, N. Nishikawa, M. Kiuchi, T. Ide, M. Shimizu, T. Inoue, and M. Hata, *Japan. J. Appl. Phys.* **52**, 08JN12 (2013).
- [25] K. Kalbarczyk, K. Dybko, K. Gas, D. Sztenkiel, M. Foltyn, M. Majewicz, P. Nowicki, E. Łusakowska, D. Hommel, and M. Sawicki, *Journal of Alloys and Compounds* **804**, 415 (2019).
- [26] A. Wołoś, M. Palczewska, M. Zajac, J. Gosk, M. Kamińska, A. Twardowski, M. Bockowski, I. Grzegory, and S. Porowski, *Phys. Rev. B* **69**, 115210 (2004).
- [27] E. Piskorska-Hommel, M. J. Winiarski, G. Kunert, I. N. Demchenko, O. D. Roshchupkina, J. Grenzer, J. Falta, D. Hommel, and V. Holý, *Journal of Applied Physics* **117**, 065702 (2015), <https://doi.org/10.1063/1.4907583>.
- [28] L. Janicki, G. Kunert, M. Sawicki, E. Piskorska-Hommel, K. Gas, R. Jakiela, D. Hommel, and R. Kudrawiec, *Scientific Reports* **7**, 41877 (2017).
- [29] J. Blinowski, P. Kacman, and J. A. Majewski, *Phys. Rev. B* **53**, 9524 (1996).
- [30] H. Morkoc, *Handbook of nitride semiconductors and devices: electronic and optical processes in nitrides* (Wiley-VCH Verlag GmbH, Weinheim 63 (1), 2009) pp. 419–425.
- [31] H. Amano, Y. Baines, E. Beam, M. Borga, T. Bouchet, P. R. Chalker, M. Charles, K. J. Chen, N. Chowdhury, R. Chu, C. D. Santi, M. M. D. Souza, S. Decoutere, L. D. Cioccio, B. Eckardt, T. Egawa, P. Fay, J. J. Freedman, L. Guido, O. Häberlen, G. Haynes, T. Heckel, D. Hemakumara, P. Houston, J. Hu, M. Hua, Q. Huang, A. Huang, S. Jiang, H. Kawai, D. Kinzer, M. Kuball, A. Kumar, K. B. Lee, X. Li, D. Marcon, M. März, R. McCarthy, G. Meneghesso, M. Meneghini, E. Morvan, A. Nakajima, E. M. S. Narayanan, S. Oliver, T. Palacios, D. Piedra, M. Plissonnier, R. Reddy, M. Sun, I. Thayne, A. Torres, N. Trivellin, V. Unni, M. J. Uren, M. V. Hove, D. J. Wallis, J. Wang, J. Xie, S. Yagi, S. Yang, C. Youtsey, R. Yu, E. Zanoni, S. Zeltner, and Y. Zhang, *Journal of Physics D: Applied Physics* **51**, 163001 (2018).
- [32] K. Gas and M. Sawicki, *Measurement Science and Technology* **30**, 085003 (2019).
- [33] R. Wilson, F. Stevie, and C. Magee, *Secondary Ion Mass Spectrometry: A Practical Handbook for Depth Profiling and Bulk Impurity Analysis* (Wiley, 1989).
- [34] W. Stefanowicz, D. Sztenkiel, B. Faina, A. Grois, M. Rovezzi, T. Devillers, A. Navarro-Quezada, T. Li, R. Jakiela, M. Sawicki, T. Dietl, and A. Bonanni, *Phys. Rev. B* **81**, 235210 (2010).
- [35] D. Sztenkiel, M. Foltyn, G. P. Mazur, R. Adhikari, K. Kosił, K. Gas, M. Zgierski, R. Kruszka, R. Jakiela, T. Li, A. Piotrowska, A. Bonanni, M. Sawicki, and T. Dietl, *Nature Communications* **7**, 13232 (2016).
- [36] D. Sztenkiel, K. Gas, J. Domagala, D. Hommel, and M. Sawicki, *New Journal of Physics* **X**, YY (2020).
- [37] J. Gosk, M. Zajac, A. Wołoś, M. Kamińska, A. Twardowski, I. Grzegory, M. Bockowski, and S. Porowski, *Phys. Rev. B* **71**, 094432 (2005).
- [38] A. Bonanni, M. Sawicki, T. Devillers, W. Stefanowicz, B. Faina, T. Li, T. E. Winkler, D. Sztenkiel, A. Navarro-Quezada, M. Rovezzi, R. Jakiela, A. Grois, M. Wegscheider, W. Jantsch, J. Suffczyński, F. D'Acapito, A. Meingast, G. Kothleitner, and T. Dietl, *Phys. Rev. B* **84**, 035206 (2011).
- [39] K. Gas, J. Z. Domagala, R. Jakiela, G. Kunert, P. Dłuzewski, E. Piskorska-Hommel, W. Paszkowicz, D. Sztenkiel, M. J. Winiarski, D. Kowalska, R. Szukiewicz, T. Baraniecki, A. Miszczuk, D. Hommel, and M. Sawicki, *Journal of Alloys and Compounds* **747**, 946 (2018).
- [40] M. Sawicki, W. Stefanowicz, and A. Ney, *Semicon. Sci. Technol.* **26**, 064006 (2011).
- [41] L. M. C. Pereira, *Journal of Physics D: Applied Physics* **50**, 393002 (2017).
- [42] H. Przybylińska, A. Bonanni, A. Wołos, M. Kiecana, M. Sawicki, T. Dietl, H. Malissa, C. Simbrunner, M. Wegscheider, H. Sitter, K. Rumpf, P. Granitzer, H. Krenn, and W. Jantsch, *Materials Science and Engineering: B* **126**, 222 (2006), eMRS 2005, Symposium B, Spintronics.
- [43] A. Navarro-Quezada, M. Aiglinger, B. Faina, K. Gas, M. Matzer, T. Li, R. Adhikari, M. Sawicki, and A. Bonanni, *Phys. Rev. B* **99**, 085201 (2019).
- [44] G. P. Mazur, K. Dybko, A. Szczerbakow, J. Z. Domagala, A. Kazakov, M. Zgierski, E. Łusakowska, S. Kret, J. Korczak, T. Story, M. Sawicki, and T. Dietl, *Phys. Rev. B* **100**, 041408 (2019).
- [45] M. Wang, C. Andrews, S. Reimers, O. J. Amin, P. Wadley, R. P. Campion, S. F. Poole, J. Felton, K. W. Edmonds, B. L. Gallagher, A. W. Rushforth, O. Makarovskiy, K. Gas, M. Sawicki, D. Kriegner, J. Zubáč, K. Olejník, V. Novák, T. Jungwirth, M. Shahrokhand, U. Zeitler, S. S. Dhesi, and F. Maccheronzi, *Phys. Rev. B* **101**, 094429 (2020).

- [46] L. Scheffler, K. Gas, S. Banik, M. Kamp, J. Knobel, H. Lin, C. Schumacher, C. Gould, M. Sawicki, J. Kleinlein, and L. W. Molenkamp, *Phys. Rev. Materials* **4**, 114402 (2020).
- [47] K. Gas, D. Hommel, and M. Sawicki, *Journal of Alloys and Compounds* **817**, 152789 (2020).
- [48] P. Stamenov and J. M. D. Coey, *Review of Scientific Instruments* **77**, 015106 (2006), <https://doi.org/10.1063/1.2149190>.
- [49] M. Zajac, J. Gosk, M. Kamińska, A. Twardowski, T. Szyszko, and S. Podsiadło, *Appl. Phys. Lett.* **79**, 2432 (2001).
- [50] S. Granville, B. J. Ruck, F. Budde, H. J. Trodahl, and G. V. M. Williams, *Phys. Rev. B* **81**, 184425 (2010).
- [51] P. W. Anderson, *Phys. Rev.* **79**, 350 (1950).
- [52] J. B. Goodenough, *J. Phys. Chem. Solids* **6**, 287 (1958).
- [53] J. Kanamori, *J. Phys. Chem. Solids* **10**, 87 (1959).
- [54] W. Mac, A. Twardowski, P. J. T. Eggenkamp, H. J. M. Swagten, Y. Shapira, and M. Demianiuk, *Phys. Rev. B* **50**, 14144 (1994).
- [55] A. Twardowski, T. Fries, Y. Shapira, P. Eggenkamp, H. J. M. Swagten, and M. Demianiuk, *J. Appl. Phys.* **73**, 5745 (1993).
- [56] M. Herbich, W. Mac, A. Twardowski, K. Ando, Y. Shapira, and M. Demianiuk, *Phys. Rev. B* **58**, 1912 (1998).
- [57] A. Wołoś, A. Wyszomolek, M. Kamińska, A. Twardowski, M. Bockowski, I. Grzegory, S. Porowski, and M. Potemski, *Phys. Rev. B* **70**, 245202 (2004).
- [58] A. Savoyant, A. Stepanov, R. Kuzian, C. Deparis, C. Morhain, and K. Graszka, *Phys. Rev. B* **80**, 115203 (2009).
- [59] C. Rudowicz, K. Tadyszak, and T. Ślusarski, *J. Magn. Magn. Mat.* **485**, 381 (2019).
- [60] Y. Shapira and V. Bindilatti, *J. Appl. Phys.* **92**, 4155 (2002).
- [61] Simserides, C., Majewski, J.A., Trohidou, K.N., and Dietl, T., *EPJ Web of Conferences* **75**, 01003 (2014).
- [62] M. Bockowski, M. Iwinska, M. Amilusik, B. Lucznik, M. Fijalkowski, E. Litwin-Staszewska, R. Piotrkowski, and T. Sochacki, *Journal of Crystal Growth* **499**, 1 (2018).
- [63] M. Iwinska, M. Zajac, B. Lucznik, M. Fijalkowski, M. Amilusik, T. Sochacki, E. Litwin-Staszewska, R. Piotrkowski, I. Grzegory, and M. Bockowski, *Japanese Journal of Applied Physics* **58**, SC1047 (2019).